Available online at www.sciencedirect.com
ScienceDirect
Journal of Process Control 18 (2008) 753–768
JOURNAL OF PROCESS CONTROL
www.elsevier.com/locate/jprocont

Applying the unscented Kalman filter for nonlinear state estimation

Rambabu Kandepu [a], Bjarne Foss [a,*], Lars Imsland [b]

[a] Department of Engineering Cybernetics, Norwegian University of Science and Technology, Trondheim 7491, Norway
[b] SINTEF ICT, Trondheim 7465, Norway

Received 9 July 2007; accepted 4 November 2007

Abstract

Based on presentation of the principles of the EKF and UKF for state estimation, we discuss the differences of the two approaches. Four rather different simulation cases are considered to compare the performance. A simple procedure to include state constraints in the UKF is proposed and tested. The overall impression is that the performance of the UKF is better than the EKF in terms of robustness and speed of convergence. The computational load in applying the UKF is comparable to the EKF.

Keywords: Nonlinear state estimation; Kalman filter; Constraint handling

1. Introduction

In the process industries one of the main goals is to make the end product at the lowest possible cost while satisfying product quality constraints. State estimation often play an important role in accomplishing this goal in process control and performance monitoring applications. There are many uncertainties to deal with in process control; model uncertainties, measurement uncertainties and uncertainties in terms of different noise sources acting on the system. In this kind of environment, representing the model state by an (approximated) probability distribution function (pdf) has distinct advantages. State estimation is a means to propagate the pdf of the system states over time in some optimal way. It is most common to use the Gaussian pdf to represent the model state, process and measurement noises. The Gaussian pdf can be characterized by its mean and covariance. The Kalman filter (KF) propagates the mean and covariance of the pdf of the model state in an optimal (minimum mean square error) way in case of linear dynamic systems [2,11].

All practical systems posses some degree of nonlinearity. Depending on the type of process and the operating region of the process, some processes can be approximated with a linear model and the KF can be used for state estimation. In some cases the linear approximation may not be accurate enough, and state estimator designs using nonlinear process models are necessary. The most common way of applying the KF to a nonlinear system is in the form of the extended Kalman filter (EKF). In the EKF, the pdf is propagated through a linear approximation of the system around the operating point at each time instant. In doing so, the EKF needs the Jacobian matrices which may be difficult to obtain for higher order systems, especially in the case of time-critical applications. Further, the linear approximation of the system at a given time instant may introduce errors in the state which may lead the state to diverge over time. In other words, the linear approximation may not be appropriate for some systems. In order to overcome the drawbacks of the EKF, other nonlinear state estimators have been developed such as the unscented Kalman filter (UKF) [1], the ensemble Kalman filter (EnKF)[10] and high order EKFs. The EnKF is especially designed for large scale systems, for instance, oceanographic models and reservoir models [10]. The UKF seems to be a promising alternative for process control applications [15,16,20].

* Corresponding author. Tel.: +47 73594476; fax: +47 73594599.
E-mail address: Bjarne.Foss@itk.ntnu.no (B. Foss).

0959-1524/$ - see front matter © 2007 Elsevier Ltd. All rights reserved.
doi:10.1016/j.jprocont.2007.11.004

The UKF propagates the pdf in a simple and effective way and it is accurate up to second order in estimating mean and covariance [1]. The present paper focuses on using the UKF for nonlinear state estimation in process systems and the performance is evaluated in comparison with the EKF. The paper proposes a simple method to incorporate state constraints in the UKF.

Section 2 describes the principles and algorithms of EKF and UKF. Section 3 introduces a method to incorporate the state constraints in the UKF state estimation and compares it with the EKF. Four examples are studied in Section 4 to compare the performances of the UKF and EKF. Discussion on the differences between the UKF and EKF is presented in Section 5 and conclusions are drawn in Section 6.

2. The EKF and UKF algorithms for nonlinear state estimation

We present the principles and algorithms of the EKF and UKF. At the end of the section, different characteristics of the EKF and UKF are compared.

2.1. EKF principle and algorithm

To illustrate the principle behind the EKF, consider the following example. Let $x \in \mathbb{R}^n$ be a random vector and

$$y = g(x) \tag{1}$$

be a nonlinear function, $g : \mathbb{R}^n \to \mathbb{R}^m$. The question is how to compute the pdf of y given the pdf of x? For example, in the case of being Gaussian, how to calculate the mean ($\overline{y}$) and covariance (Σ_y) of y? If g is a linear function and the pdf of x is a Gaussian distribution, then Kalman filter (KF) is optimal in propagating the pdf. Even if the pdf is not Gaussian, the KF is optimal up to the first two moments in the class of linear estimators [9]. The KF is extended to the class of nonlinear systems termed EKF, by using linearization. In the case of a nonlinear function ($g(x)$), the nonlinear function is linearized around the current value of x, and the KF theory is applied to get the mean and covariance of y. In other words, the mean ($\overline{y}^{\mathrm{EKF}}$) and covariance ($P_y^{\mathrm{EKF}}$) of y, given the mean ($\overline{x}$) and covariance (P_x) of the pdf of x are calculated as follows:

$$\overline{y}^{\mathrm{EKF}} = g(\overline{x}), \tag{2}$$

$$P_y^{\mathrm{EKF}} = (\nabla g) P_x (\nabla g)^{\mathrm{T}}, \tag{3}$$

where (∇g) is the Jacobian of $g(x)$ at $\overline{x}$.

Algorithm. Let a general nonlinear system be represented by the following standard discrete time equations:

$$x_k = f(x_{k-1}, v_{k-1}, u_{k-1}), \tag{4}$$

$$y_k = h(x_k, n_k, u_k), \tag{5}$$

where $x \in \mathbb{R}^{n_x}$ is the system state, $v \in \mathbb{R}^{n_v}$ the process noise, $n \in \mathbb{R}^{n_n}$ the observation noise, u the input and y the noisy observation of the system. The nonlinear functions f and h are need not necessarily be continuous. The EKF algorithm for this system is presented below:

- *Initialization at* $k = 0$:

$$\widehat{x}_0 = E[x_0],$$
$$P_{x_0} = E[(x_0 - \widehat{x}_0)(x_0 - \widehat{x}_0)^{\mathrm{T}}],$$
$$P_v = E[(v - \overline{v})(v - \overline{v})^{\mathrm{T}}],$$
$$P_n = E[(n - \overline{n})(n - \overline{n})^{\mathrm{T}}].$$

- *For* $k = 1, 2, \ldots, \infty$:

(1) Prediction step.

(a) Compute the process model Jacobians:

$$F_{x_k} = \nabla_x f(x, \overline{v}, u_{k-1})|_{x=\widehat{x}_{k-1}},$$
$$G_v = \nabla_v f(\widehat{x}_{k-1}, v, u_k)|_{v=\overline{v}}.$$

(b) Compute predicted state mean and covariance (*time update*)

$$\widehat{x}_k^- = f(\widehat{x}_{k-1}, \overline{v}, u_k),$$
$$P_{x_k}^- = F_{x_k} P_{x_k} F_{x_k}^{\mathrm{T}} + G_v P_v G_v^{\mathrm{T}}.$$

(2) Correction step.

(a) Compute observation model Jacobians:

$$H_{x_k} = \nabla_x h(x, \overline{n}, u_k)|_{x=\widehat{x}_k^-},$$
$$D_n = \nabla_n h(\widehat{x}_k^-, n, u_k)|_{n=\overline{n}}.$$

(b) Update estimates with latest observation (*measurement update*)

$$K_k = P_{x_k}^- H_{x_k}^{\mathrm{T}} (H_{x_k} P_{x_k}^- H_{x_k}^{\mathrm{T}} + D_n P_n D_n^{\mathrm{T}})^{-1},$$
$$\widehat{x}_k = \widehat{x}_k^- + K_k[y_k - h(\widehat{x}_k^-, \overline{n})],$$
$$P_{x_k} = (I - K_k H_{x_k}) P_{x_k}^-.$$

2.2. UKF principle and algorithm

Consider now the same example as in the previous section. The question is how the UKF compute pdf of y given the pdf of x, in other words, how to calculate the mean ($\overline{y}^{\mathrm{UKF}}$) and covariance ($P_y^{\mathrm{UKF}}$) of y, in the case of being Gaussian? Consider a set of points

$$x^{(i)}, \quad i \in \{1, \ldots, p\}, \; p = 2n + 1,$$

(similar to the random samples of a specific distribution function in Monte Carlo simulations) with each point being associated with a weight $w^{(i)}$. These sample points are termed as sigma points. Then the following steps are involved in approximating the mean and covariance: Propagate each sigma point through the nonlinear function,

$$y^{(i)} = g(x^{(i)})$$

- the mean is approximated by the weighted average of the transformed points,

$$\overline{y}^{\mathrm{UKF}} = \sum_{i=0}^{p} w^{(i)} y^{(i)}, \ \Sigma w^{(i)} = 1$$

- and the covariance is computed by the weighted outer product of the transformed points,

$$P_y^{\mathrm{UKF}} = \sum_{i=0}^{p} w^{(i)} (y^{(i)} - \overline{y})(y^{(i)} - \overline{y})^{\mathrm{T}}.$$

Both the sigma points and the weights are computed deterministically through a set of conditions given in [1].

Algorithm. The UKF algorithm is presented below; for background theory, refer to [1,8,9]. Let the system be represented by (4) and (5). An augmented state at time instant k,

$$x_k^a \triangleq \begin{bmatrix} x_k \\ v_k \\ n_k \end{bmatrix} \tag{6}$$

is defined. The augmented state dimension is,

$$N = n_x + n_v + n_n \tag{7}$$

Similarly, the augmented state covariance matrix is built from the covariance matrices of x, v and n,

$$P^a \triangleq \begin{bmatrix} P_x & 0 & 0 \\ 0 & P_v & 0 \\ 0 & 0 & P_n \end{bmatrix} \tag{8}$$

where P_v and P_n are the process and observation noise covariance matrices.

- *Initialization at* $k = 0$:

$$\widehat{x}_0 = E[x_0], \quad P_{x_0} = E[(x_0 - \widehat{x}_0)(x_0 - \widehat{x}_0)^{\mathrm{T}}]$$
$$\widehat{x}_0^a = E[x^a] = E[\widehat{x}_0 \quad 0 \quad 0]^{\mathrm{T}}$$
$$P_0^a = E[(x_0^a - \widehat{x}_0^a)(x_0^a - \widehat{x}_0^a)^{\mathrm{T}}] = \begin{bmatrix} P_x & 0 & 0 \\ 0 & P_v & 0 \\ 0 & 0 & P_n \end{bmatrix}$$

- *For* $k = 1, 2, \ldots, \infty$:

(1) Calculate $2N + 1$ sigma-points based on the present state covariance:

$$\mathbf{X}_{i,k-1}^a \begin{cases} \triangleq \widehat{x}_{k-1}^a, & i = 0, \\ \triangleq \widehat{x}_{k-1}^a + \gamma \mathbf{S}_i, & i = 1, \ldots, N, \\ \triangleq \widehat{x}_{k-1}^a - \gamma \mathbf{S}_i, & i = N+1, \ldots, 2N, \end{cases} \tag{9}$$

where $\mathbf{S}_i$ is the ith column of the matrix,

$S = \sqrt{P_{k-1}^a}$.

In (9) γ is a scaling parameter [8],

$\gamma = \sqrt{N + \lambda}, \quad \lambda = \alpha^2(N + \kappa) - N,$

where α and κ are tuning parameters. We must choose $\kappa \geqslant 0$, to guarantee the semi-positive definiteness of the covariance matrix, a good default choice is $\kappa = 0$. The parameter α, $0 \leqslant \alpha \leqslant 1$, controls the size of the sigma-point distribution and it should ideally be a small number [8].The ith sigma point (augmented) is the ith column of the sigma point matrix,

$$\mathbf{X}_{i,k-1}^a = \begin{bmatrix} \mathbf{X}_{i,k-1}^x \\ \mathbf{X}_{i,k-1}^v \\ \mathbf{X}_{i,k-1}^n \end{bmatrix},$$

where the superscripts x, v and n refer to a partition conformal to the dimensions of the state, process noise and measurement noise, respectively.

(2) Time-update equations:
Transform the sigma points through the state-update function,

$$\mathbf{X}_{i,k/k-1}^x = f(\mathbf{X}_{i,k-1}^x, \mathbf{X}_{i,k-1}^v, u_{k-1}), \quad i = 0, 1, \ldots, 2N. \tag{10}$$

Calculate the apriori state estimate and apriori covariance,

$$\widehat{x}_k^- = \sum_{i=0}^{2N} (w_{\mathrm{m}}^{(i)} \mathbf{X}_{i,k/k-1}^x), \tag{11}$$

$$P_{x_k}^- = \sum_{i=0}^{2N} w_{\mathrm{c}}^{(i)} (\mathbf{X}_{i,k/k-1}^x - \widehat{x}_k^-)(\mathbf{X}_{i,k/k-1}^x - \widehat{x}_k^-)^{\mathrm{T}}. \tag{12}$$

The weights $w_{\mathrm{m}}^{(i)}$ and $w_{\mathrm{c}}^{(i)}$ are defined as,

$$w_{\mathrm{m}}^{(0)} = \frac{\lambda}{N + \lambda}, \quad i = 0,$$
$$w_{\mathrm{c}}^{(0)} = \frac{\lambda}{N + \lambda} + (1 - \alpha^2 + \beta), \quad i = 0,$$
$$w_{\mathrm{m}}^{(i)} = w_{\mathrm{c}}^{(i)} = \frac{1}{2(N + \lambda)}, \quad i = 1, \ldots, 2N,$$

where β is a non-negative weighting parameter introduced to affect the weighting of the zeroth sigma-point for the calculation of the covariance. This parameter (β) can be used to incorporate knowledge of the higher order moments of the distribution. For a Gaussian prior the optimal choice is $\beta = 2$ [8].

(3) Measurement-update equations:
Transform the sigma points through the measurement-update function,

$$\mathbf{Y}_{i,k/k-1} = h(\mathbf{X}_{i,k/k-1}^x, \mathbf{X}_{k-1}^n, u_k), \quad i = 0, 1, \ldots, 2N \tag{13}$$

and the mean and covariance of the measurement vector is calculated,

$$\widehat{y}_k^- = \sum_{i=0}^{2N} w_{\mathrm{m}}^{(i)} \mathbf{Y}_{i,k/k-1},$$

$$P_{\overline{y}_k} = \sum_{i=0}^{2N} w_{\mathrm{c}}^{(i)} (\mathbf{Y}_{i,k/k-1} - \widehat{y}_k^-)(\mathbf{Y}_{i,k/k-1} - \widehat{y}_k^-)^{\mathrm{T}}.$$

The cross covariance is calculated according to

$$P_{x_k y_k} = \sum_{i=0}^{2N} w_c^{(i)} (\mathbf{X}^x_{i,k/k-1} - \widehat{x}_k^-)(\mathbf{Y}_{i,k/k-1} - \widehat{y}_k^-)^{\mathrm{T}}.$$

The Kalman gain is given by,

$$K_k = P_{x_k y_k} P_{\bar{y}_k}^{-1},$$

and the UKF estimate and its covariance are computed from the standard Kalman update equations,

$$\widehat{x}_k = \widehat{x}_k^- + K_k(y_k - \widehat{y}_k^-),$$
$$P_{x_k} = P_{x_k}^- - K_k P_{\bar{y}_k} K_k^{\mathrm{T}}. \quad (14)$$

2.3. Discussion

The difference in the principles of state estimation using UKF and EKF is illustrated based the Fig. 1 by considering the following example,

$$y = g(x) = x^2, \quad x \in \mathbb{R}, \quad \bar{x} = X_{\mathrm{mean}} = 6, \quad \Sigma_x = 16.$$

The figure illustrates how the mean and variance of x are propagated to obtain mean and variance of y for EKF and UKF. The true mean and variance are calculated by using the following equations,

$$Y^{\mathrm{true}}_{\mathrm{mean}} = E[g(x)] = \int_{-\infty}^{\infty} x^2 . \frac{1}{\sqrt{2\pi}\sigma} \mathrm{e}^{-\frac{1}{2}\left(\frac{x-\bar{x}}{\sigma}\right)^2} \mathrm{d}x,$$
$$P_y^{\mathrm{true}} = E[(g(x) - E[g(x)])^2].$$

where $\sigma = \sqrt{\Sigma_x}$ is the standard deviation. The true mean and variance are 51.43 and 2686, respectively. The EKF mean is obtained by using (2) giving

$$Y^{\mathrm{EKF}}_{\mathrm{mean}} = 36.00,$$

and the variance is obtained by performing the linearization as shown in the figure and using (3),

$$P_y^{\mathrm{EKF}} = 2304.$$

For the UKF, three sigma points are propagated through the function, and the mean and variance are calculated accordingly,

$$Y^{\mathrm{UKF}}_{\mathrm{mean}} = 52.00,$$
$$P_y^{\mathrm{UKF}} = 2816.$$

The UKF approximates the propagation of the pdf through the nonlinearity more accurately when compared to the EKF as illustrated by the numbers in the example above.

In the EKF algorithm, during the time-update (prediction) step, the mean is propagated through the nonlinear function, in other words, this introduces an error since in general $\bar{y} \neq g(\bar{x})$. In case of the UKF, during the time-update step, all the sigma points are propagated through the nonlinear function which makes the UKF a better and more effective nonlinear approximator. The UKF principle is simple and easy to implement as it does not require the calculation of Jacobians at each time step. The UKF is accurate up to second order moments in the pdf propagation where as the EKF is accurate up to first order moment [8].

Later, we will see that it is possible to implement state constraints by proper conditioning of the sigma points. An example (state estimation of a reversible reaction) will be considered to illustrate the constraint handling capability of the UKF.

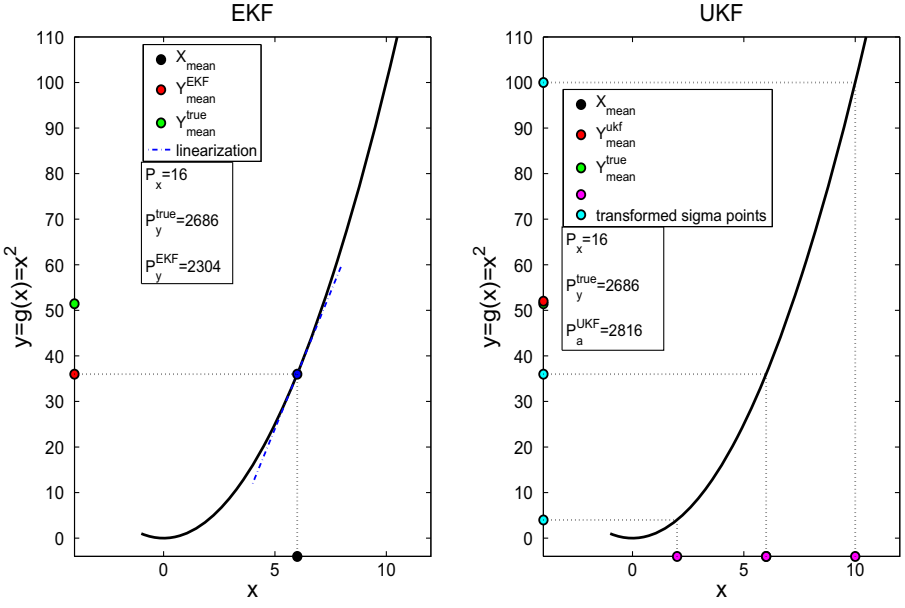

Fig. 1. Illustration of principle of EKF and UKF.

3. State estimation with constraints

Constraints on states to be estimated are important model information that is often not used in state estimation. Typically, such constraints are due to physical limitations on the states; for instance, estimated concentrations should remain positive. In Kalman filter theory, there is no general way of incorporating these constraints into the estimation problem. However, the constraints can be incorporated in the KF by projecting the unconstrained KF estimates onto the boundary of the feasible region at each time step [18,19]. An other way of nonlinear state estimation with constraints is moving horizon estimation (MHE), in which the constraints can be included in the estimation problem in a natural way [17]. In MHE, the state trajectory is computed taking state constraints into account at the expense of solving a nonlinear programing problem at each time step. The numerical optimization at each time step may be a challenge in time-critical applications. In this section, a new and simple method is introduced to handle state constraints in the UKF and it is compared to the standard way of constraint handling in the EKF, known as 'clipping' [14].

Assume that the state constraints are represented by box constraints,

$$x_L \leqslant x \leqslant x_H.$$

We will illustrate the method for $x \in \mathbb{R}^2$. In case of a second order system, the feasible region by the box constraints can be represented by a rectangle as in Fig. 2. The figure shows the illustration of the steps of constraint handling in case of the EKF and UKF from one time step to the

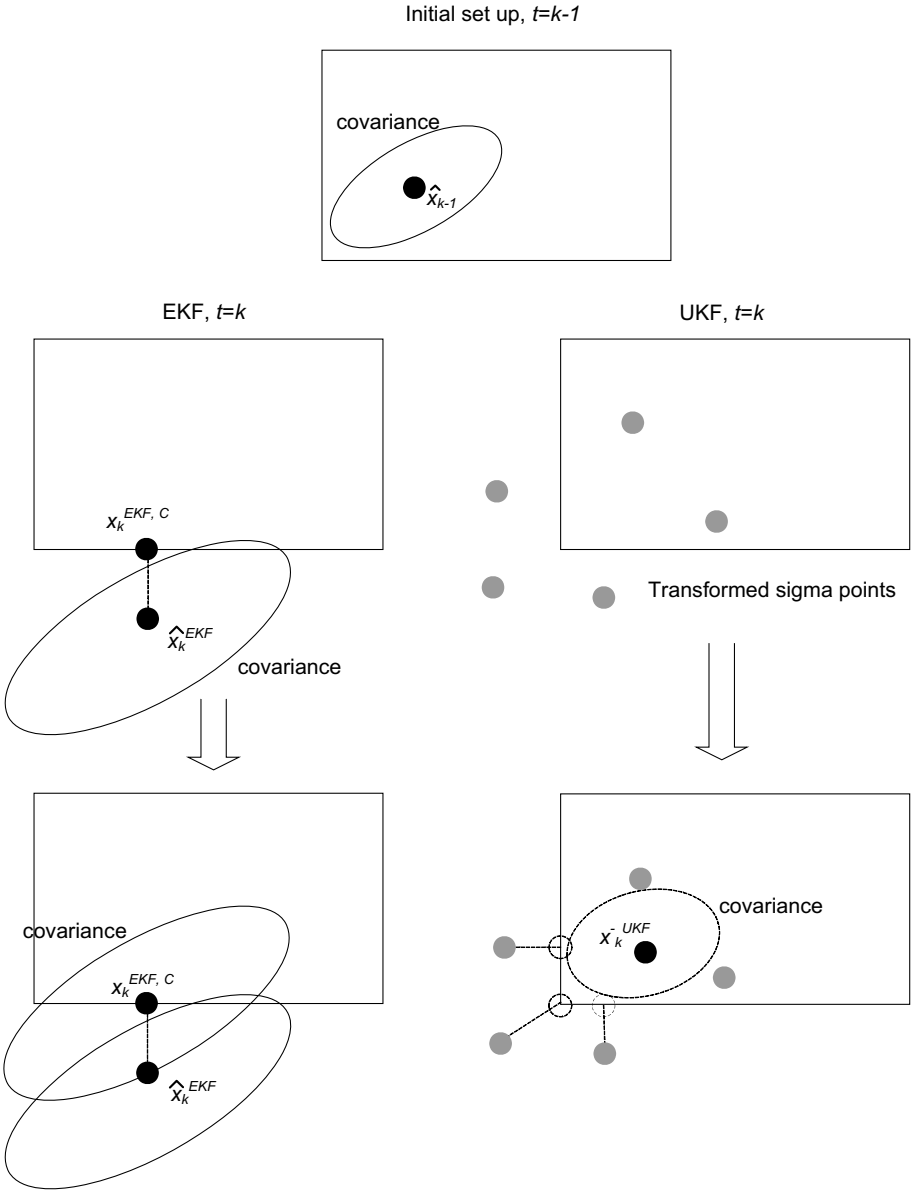

Fig. 2. Illustration of estimation with state constraints.

next. At $t = k-1$, the true state (x_k), its estimate ($\hat{x}_k$) and state covariance are selected as shown in the figure. At $t = k$, the unconstrained EKF estimate ($\hat{x}_k^{\mathrm{EKF}}$) is outside the feasible region and is projected to the boundary of the feasible region to get the constrained EKF estimate ($x_k^{\mathrm{EKF,C}}$) as shown in the figure. While projecting the EKF estimate, the covariance of the EKF estimate is not changed and thus the constraints have no effect on the covariance. Hence, the covariance does not include any constraint information. This way of the handling constraints in the EKF is termed as 'clipping' in literature [14].

The constraints information can be incorporated in the UKF algorithm in a simple way during the time-update step. After the propagation of the sigma points from (10), the (unconstrained) transformed sigma points which are outside the feasible region can be projected onto the boundary of the feasible region and continue the further steps. In Fig. 2, at $t = k$ three sigma points which are outside the feasible region are projected onto the boundary (lower right plot in the figure). The mean and covariance with the constrained sigma points now represents the apriori UKF estimate ($x_k^{\mathrm{UKF}^-}$) and covariance, and they are further updated in the measurement-update step. The advantage here is that the new apriori covariance includes information on the constraints, which should make the UKF estimate more efficient (accurate) compared to the EKF estimate. An example (reversible reaction) is considered in the next section to illustrate the state estimation with constraints with the proposed method.

Extension of the proposed method to higher dimension is straightforward. Alternative linear constraints, e.g.,

$$Cx \leqslant d$$

are easily included by projecting the sigma point violating the inequality normally onto the boundary of feasible region. It is observed that the new (constrained) covariance obtained at a time step is lower in size compared to the unconstrained covariance. If, in case, the estimate after the measurement-update (refer (14)) is outside the feasible region, the same projection technique can be extended. Further, the technique can be extended to the sigma points from (9).

The proposed algorithm is outlined below:

Algorithm (*outline*). •*For* $k = 1, 2, \ldots \infty$:

(1) Calculate $2N+1$ sigma points based on the present state covariance according to (9) and project the sigma points which are outside the feasible region to the boundary to obtain the constrained sigma points,

$$\mathbf{X}_{i,k-1}^{x,\mathrm{C}} = P(\mathbf{X}_{i,k-1}^{x}) \quad i = 0, 1, \ldots, 2N,$$

where P refers to the projections.

(2) Time-update equations: Transform the sigma points through the state-update function,

$$\mathbf{X}_{i,k/k-1}^{x} = f(\mathbf{X}_{i,k-1}^{x,\mathrm{C}}, \mathbf{X}_{i,k-1}^{v}, u_{k-1}), \quad i = 0, 1, \ldots, 2N.$$

Again apply the constrains on the transformed sigma points to obtain the constrained transformed sigma points,

$$\mathbf{X}_{i,k/k-1}^{x,\mathrm{C}} = P(\mathbf{X}_{i,k/k-1}^{x}) \quad i = 0, 1, \ldots, 2N.$$

Calculate the apriori state estimate and apriori covariance as given in (11) and (12) using the constrained transformed sigma points $\mathbf{X}_{i,k/k-1}^{x,\mathrm{C}}$.

(3) Measurement-update equations: Transform the constrained sigma points through the measurement-update function as in (13) and obtain the UKF estimate by following the same steps given in Section 2. If UKF estimate violates the constraints, the same projection technique can be used.

4. Simulation studies

Four rather different examples are considered to compare different characteristics of the UKF and the EKF. First, the Van der Pol oscillator is considered to study the behavior of the UKF and also to compare the robustness of the estimator due to model errors with that of the EKF. Second, an estimation problem in an induction machine is chosen to evaluate the performances for a nonlinear system. Third, state estimation of a reversible reaction is studied to illustrate the constraint handling capability of the UKF. Finally, a solid oxide fuel cell (SOFC) combined gas turbine (GT) hybrid system is considered to evaluate the performances in the case of higher order, nonlinear system.

In all the examples, the following assumptions are made:

- The measurement update frequency of the KF coincides with the system discretization sampling frequency.
- The system model and the state estimator model are the same unless otherwise specified.
- Process noise and measurement noise are applied to the system. The noise is Gaussian with zero mean value.
- The tuning parameters (the initial covariance and process and measurement noise covariances) are chosen to be the same for both the EKF and UKF.
- For UKF algorithm, α,β and κ in Section 2.2 are set to the following values,

$$\alpha = 1, \quad \beta = 2 \quad \text{and} \quad \kappa = 0.$$

4.1. Van der Pol oscillator

The Van der Pol oscillator is considered as it is a widely used example in the literature. It is highly nonlinear and, depending on the direction of time, it can exhibit both stable and unstable limit cycles [12]. In case of an unstable limit cycle, if the initial state is outside the limit cycle, it diverges and if the initial state is inside the limit cycle, it

converges to zero as time progresses. In case of stable limit cycle, any non-zero initial state converges to a stable limit cycle. First, the unstable limit cycle is considered and the initial state is chosen to be just inside the limit cycle and the initial state estimate is considered outside the limit cycle to check the convergence of the UKF and EKF estimates.

4.1.1. Unstable limit cycle

The unstable limit cycle (Van der Pol oscillator in reverse time) is represented by the following state differential equations [12]

$$\dot{x}_1 = -x_2,$$
$$\dot{x}_2 = -\mu(1 - x_1^2)x_2 + x_1, \mu = 0.2.$$

The output vector is defined as

$$y = [x_1 \quad x_2]^{\mathrm{T}}.$$

The system is discretized with a sampling interval of 0.1. Process noise with a covariance of $10^{-3}I_2$ and measurement noise with a covariance of $10^{-3}I_2$ is added to the system states and measurements, respectively. These noise characteristics are used throughout Section. 4.1.

The initial state is chosen as

$$x_0 = [1.4 \quad 0]^{\mathrm{T}},$$

which is just inside the limit cycle. The initial state estimate $(\widehat{x}_0)$ is chosen to be outside the limit cycle, and the initial state covariance matrix (P_{x_0}), R_v and R_n are chosen as

$$\widehat{x}_0 = [0 \quad 5]^{\mathrm{T}}, \tag{15}$$

$$P_{x_0} = k_x I_2, \quad R_v = k_p I_2 \quad \text{and} \quad R_n = k_n I_2, \quad \text{with}$$
$$k_x = 5,\ k_p = 10^{-3} \text{ and } k_n = 10^{-3}. \tag{16}$$

The true and estimated states using the UKF and EKF are shown in Fig. 3. The UKF estimate converges to the true state and stays with it, whereas the EKF estimate could not converge to the true state as the time progresses. Fig. 4 shows the phase portraits of the UKF and EKF estimates for the first 5 s. It also includes the corresponding covariances of UKF and EKF estimates at each second, drawn according to

$$\{x | (x - \widehat{x}_k)^{\mathrm{T}} P_{x_k}^{-1} (x - \widehat{x}_k) = 1\}.$$

The covariances may also give an idea of the distribution of the sigma points around the mean at a given time instant in the case of the UKF. The covariances of the UKF and the EKF decrease a lot between from $t = 0$ and $t = 1$ s. Further it may be observed that the later covariances for the EKF are smaller than for the UKF. The choice of P_{x_0} is reasonable here as the initial state estimate is far from the true initial state. The UKF is robust to the choices of the P_{x_0}, R_v and R_n compared to the EKF as is illustrated with the following choices,

$$k_x = 10^{-2}, \quad k_p = 10^{-3} \quad \text{and} \quad k_n = 1. \tag{17}$$

Figs. 5 and 6 show the plots and phase portraits corresponding to the choices of a small P_{x_0} and a large R_n. Even though the small P_{x_0} is a bad choice for the considered $\widehat{x}_0$, the UKF estimates are still able to converge to the true states because of the measurement correction and also due to the increase of the size of the covariance until the estimates converge to the true states. On the other hand, the EKF estimate is not converging to the true state as shown in Fig. 5. The difference can be attributed to the better nonlinear approximation by the UKF at each time step. Compared to Figs. 5 and 6, both the UKF and EKF

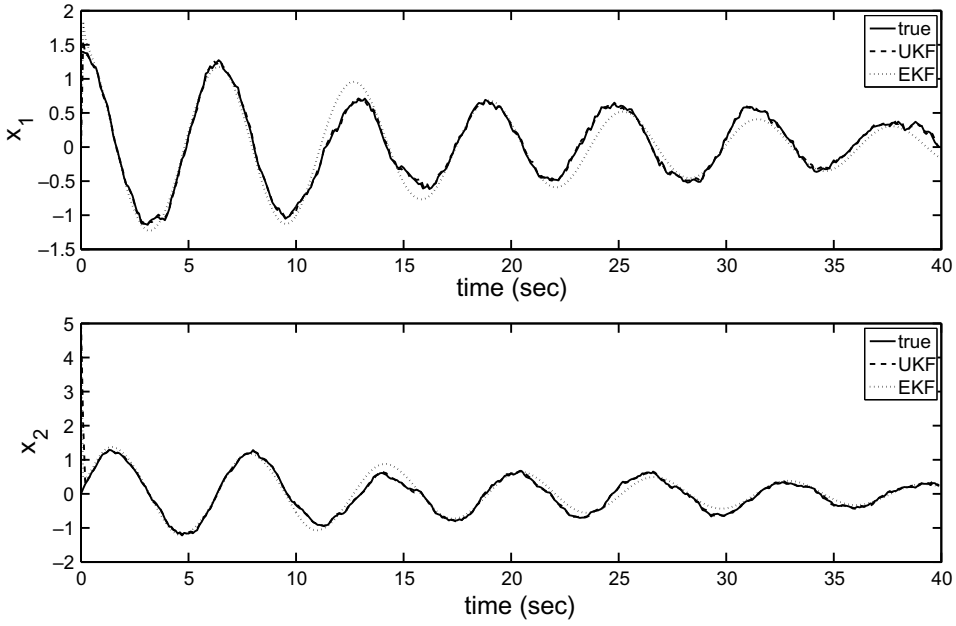

Fig. 3. Estimated states for the Van der Pol oscillator in reverse time using UKF and EKF with an initial state estimate far from the limit cycle: large initial state covariance and small measurement noise.

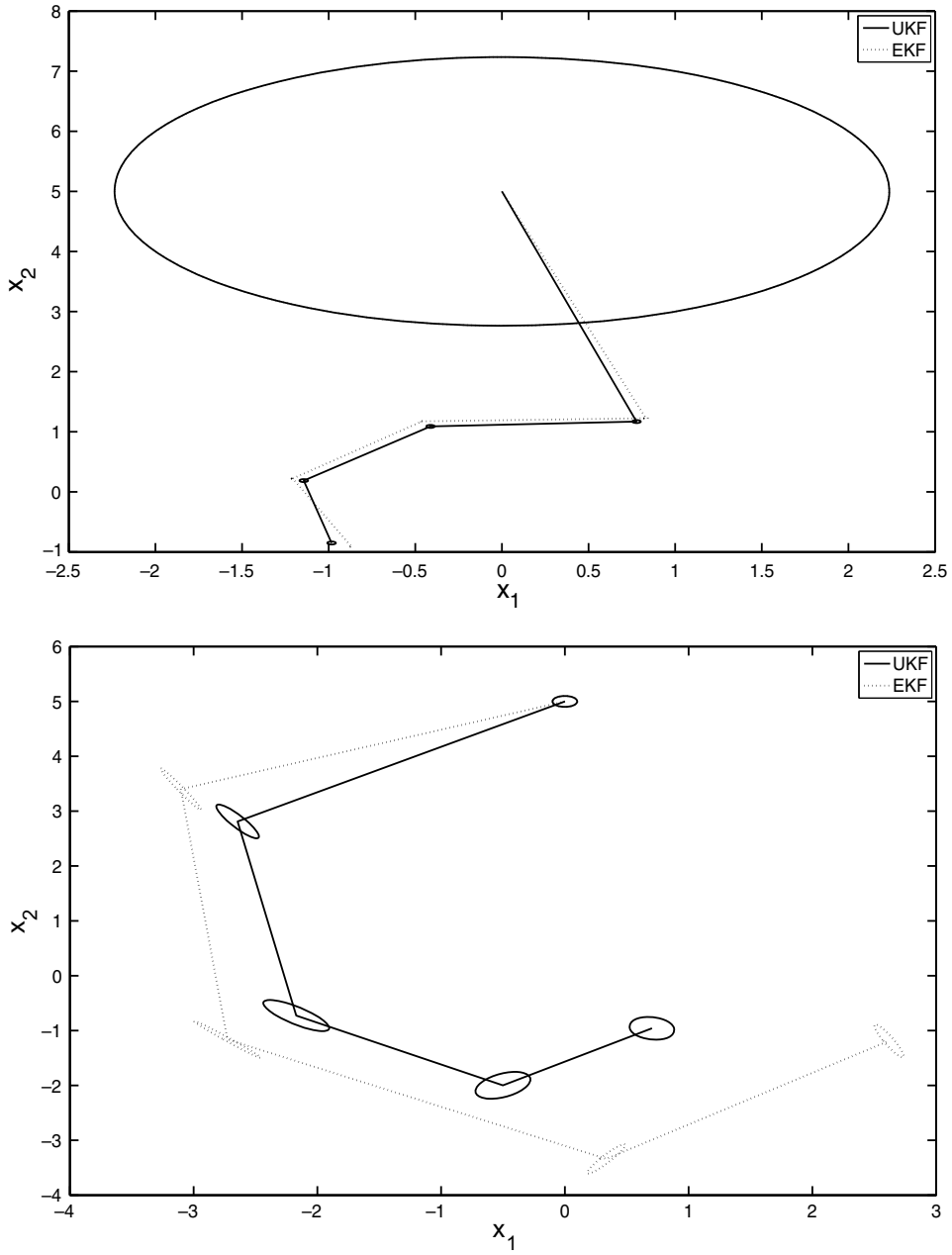

Fig. 4. Phase portraits of UKF and EKF estimates with an initial state estimate far from limit cycle, large initial state covariance matrix and small measurment noise and with covariances plotted at each second, until 5 s.

estimates converge very fast in Figs. 3 and 4. The reason is that the assumed measurement noise is less in Figs. 3 and 4, and hence the feedback in the measurement-update makes the estimates converge quite fast. In Figs. 5 and 6, the assumed measurement noise is higher meaning that the feedback from the measurement-update is less effective.

As the UKF gives a better approximation in time-update step, the UKF estimate is able to converge quite fast, even though the measurement noise is higher and the initial covariance is a bad choice. In addition, the Kalman gain is quite different in the two estimators due to the difference in the covariances as can be observed in Fig. 6. Hence, it is reasonable to assume that the correction step in the UKF also improves convergence as compared to the EKF.

To verify these results, two Monte Carlo simulations with 100 runs are performed varying the initial state, and the process and measurement noise realizations. In addition the initial state estimate is also varied. Both states of x_0 and $\widehat{x}_0$ were chosen from a normal distribution with zero mean and standard deviation 0.4. The Monte Carlo simulations differ in the choices of the tuning parameters (P_{x_0}, R_v and R_n) as given in (16) and (17). The corresponding mean square errors (MSE)s of the state estimate errors for the EKF and UKF are 0.18 and 0.02, and 0.23 and 0.09, respectively. The MSEs corresponding to the UKF

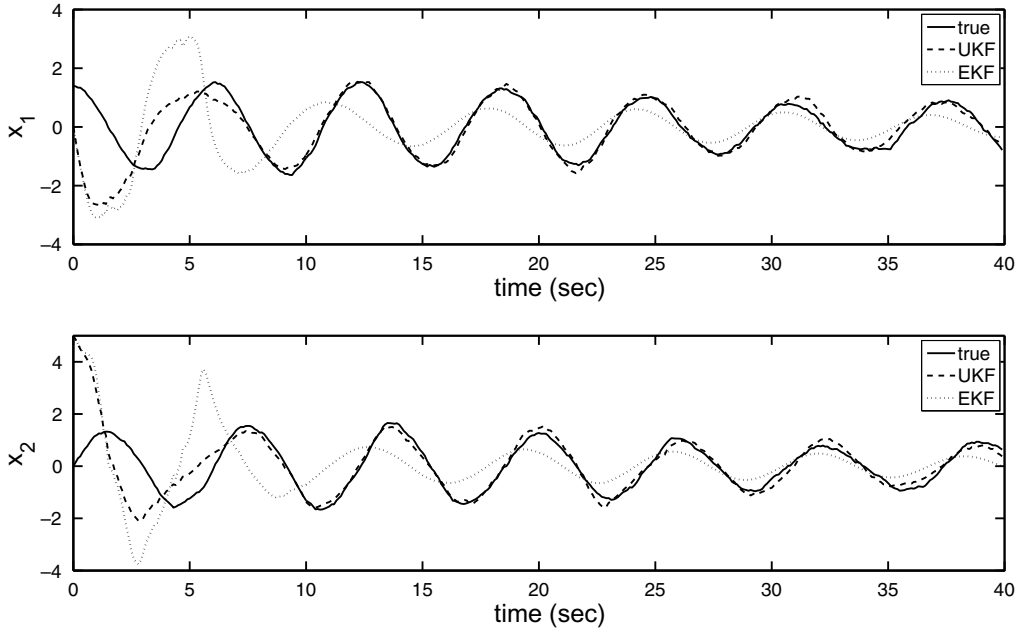

Fig. 5. Estimated states for Van der Pol equation using UKF with an initial state estimate far from limit cycle, small initial state covariance matrix and large measurment noise covariance.

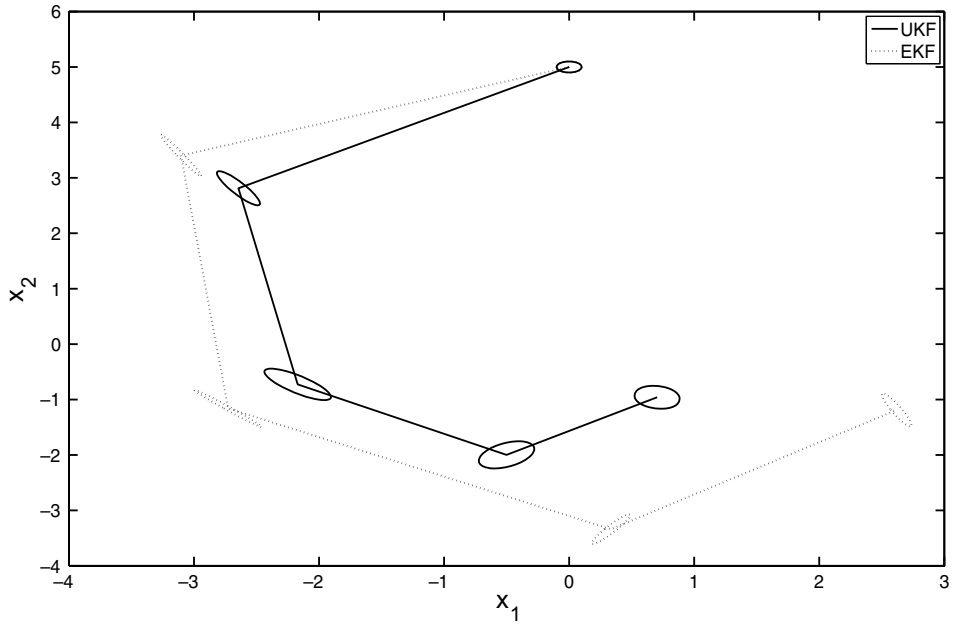

Fig. 6. Phase portraits of UKF and EKF estimates with an initial state estimate far from limit cycle, small initial state covariance matrix and large measurment noise and with covariances plotted at each second, until 5 s.

are considerably lower compared to that of EKF, and hence it can be concluded that the UKF gives improved performance compared to the EKF.

4.1.2. Stable limit cycle – with model error

In [13], it is observed that when there is a significant model error the EKF is not able to converge to the true states in case of the Van der Pol equation with a stable limit cycle. This cycle is considered to evaluate the robustness of the UKF to model errors and it is compared to that of EKF. The state and measurement equations are

$$\dot{x}_1 = x_2, \tag{18}$$

$$\dot{x}_2 = \mu(1 - x_1^2)x_2 - x_1, \quad \mu = 0.2, \tag{19}$$

$$y = [x_1 \quad x_2]^{\mathrm{T}}. \tag{20}$$

In the state estimator model the value of μ is chosen as 0.5. The system is discretized with sampling interval of 0.1. An initial state is chosen as $x_0 = [0.5 \quad 0]^T$. A initial state estimate ($\hat{x}_0$), and initial state covariance matrix (P_{x_0}), R_v and R_n are chosen as before with the following k_x, k_p and k_n values,

$$\hat{x}_0 = [5 \quad -1]^T, \quad k_x = 1, \quad k_p = 10^{-3} \quad \text{and} \quad k_n = 10^{-3}. \tag{21}$$

The estimates states using UKF and EKF are compared in Fig. 7. The errors in the estimated states in polar coordinates are shown in Fig. 8. From Figs. 7 and 8, it is clear that the EKF estimates are sensitive to the model error in μ, whereas the UKF shows robust performance to the model error.

4.2. State estimation in an induction machine

The UKF and EKF are applied to a highly nonlinear flux and angular velocity estimation problem in an induction machine. To develop high-performance induction motor drives, it may be necessary to have rotor flux estimators and rotor time constant identification schemes [3]. In [3] and [4], new EKF-based algorithms are developed for the considered estimation problem as the EKF estimator cannot produce effective results. The state space model for a symmetrical three-phase induction machine is [4],

$$\begin{aligned}
\dot{x}_1 &= k_1 x_1 + z_1 x_2 + k_2 x_3 + z_2,\\
\dot{x}_2 &= -z_1 x_1 + k_1 x_2 + k_2 x_4,\\
\dot{x}_3 &= k_3 x_1 + k_4 x_3 + (z_1 - x_5) x_4,\\
\dot{x}_4 &= k_3 x_2 - (z_1 - x_5) x_3 + k_4 x_4,\\
\dot{x}_5 &= k_5 (x_1 x_4 - x_2 x_3) + k_6 z_3,
\end{aligned} \tag{22}$$

where x_1, x_2 and x_3,x_4 are the components of the stator and the rotor flux, respectively, and x_5 is the angular velocity. All the state variables are normalized. The inputs, the frequency and the amplitude of the stator voltage are denoted by z_1 and z_2 respectively, and the load torque is denoted by z_3. $k_1, \ldots, k_6$ are parameters depending on the considered drive. The outputs are the normalized stator currents y_1 and y_2. The output equations are given by,

$$\begin{aligned}
y_1 &= k_7 x_1 + k_8 x_3,\\
y_2 &= k_7 x_2 + k_8 x_4,
\end{aligned}$$

with parameters k_7 and k_8. For simulation, the model parameters and inputs are set to the values given in Table 1. Process noise with a covariance of $10^{-4} I_5$ and measurement noise with a covariance of $10^{-2} I_2$ is added to the system states and measurements, respectively. The model is discretized with a sampling interval of 0.1.

The UKF and EKF are used to estimate the states with the actual initial condition

$$x_0 = [0.2 \quad -0.6 \quad -0.4 \quad 0.1 \quad 0.3]^T.$$

The initial estimated state is assumed to be

$$\hat{x}_0 = [0.5 \quad 0.1 \quad 0.3 \quad -0.2 \quad 4]^T.$$

The tuning parameters are selected as,

$$P_{x_0} = k_x I_5, \quad R_v = k_p I_5 \quad \text{and} \quad R_n = k_n I_2,$$
$$\text{with } k_x = 1,\ k_p = 10^{-4} \text{ and } k_n = 10^{-2}.$$

The state estimation results are shown in Fig. 9 where the UKF and EKF estimates of states x_1, x_3 and x_5 are compared with the true states. With the initial predicted state far from the actual initial state, the simulation results show that the UKF performs better than the EKF. The reason for the better performance of the UKF is attributed

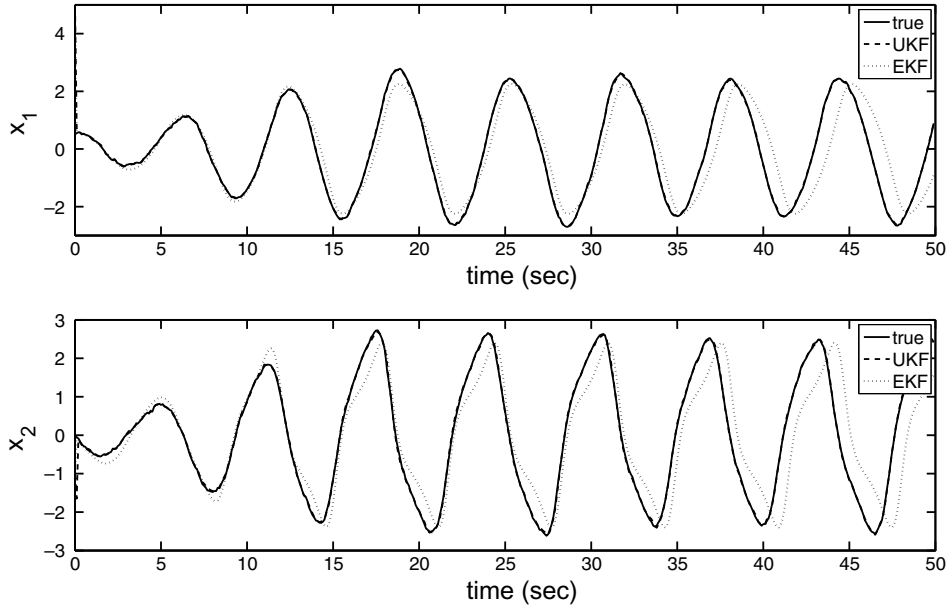

Fig. 7. Comparison of state estimates using UKF and EKF with a model error.

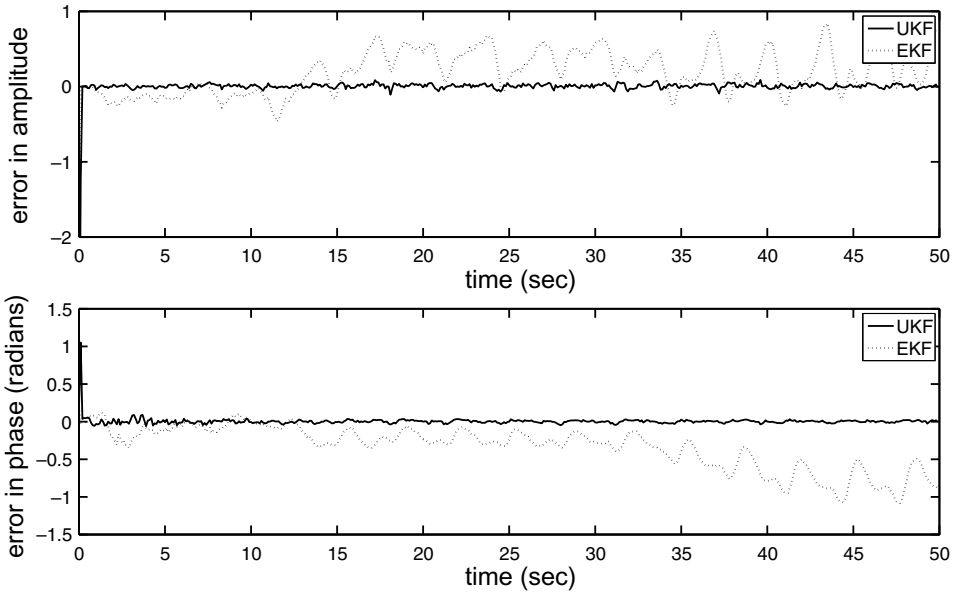

Fig. 8. Errors in amplitude and phase of the UKF and EKF state estimates.

Table 1
Model parameters and inputs

k_1	k_2	k_3	k_4	k_5	k_6	k_7	k_8	z_1	z_2	z_3
−0.186	0.178	0.225	−0.234	−0.081	4.643	−4.448	1	1	1	0

to the better nonlinear approximation at each step. It can be mentioned that the behavior of the EKF is similar to behavior observed in [3].

A Monte Carlo simulation with 100 runs was performed and the MSEs of the EKF and UKF estimates are 0.13 and 0.05, respectively. The MSE corresponding to the UKF is substantially lower compared to those of the EKF. Again the UKF performs significantly better, this time in the case of a highly nonlinear semi-realistic example.

4.3. State estimation with constraints: a reversible reaction example

We will here consider an example to illustrate the constraint handling capability of the UKF compared to that of the EKF. Consider the gas-phase, reversible reaction,

$$2A \xrightarrow{\overline{k}} B, \quad \overline{k} = 0.16,$$

with stoichiometric matrix

$$v = [-2 \quad 1]$$

and reaction rate

$$r = \overline{k} C_A^2.$$

The state and measurement vectors are defined as

$$x = \begin{bmatrix} C_A \\ C_B \end{bmatrix}, \quad y = [1 \quad 1]x,$$

where C_j denotes the concentration of species j. It is assumed that the ideal gas law holds and that the reaction occurs in a well-mixed isothermal batch reactor. Then, from first principles, the model for this system is

$$\dot{x} = f(x) = v^{\mathrm{T}} r.$$

The system is discretized with sampling interval of 0.1. The UKF and EKF are used for state estimation, with the following setup as used in [14]:

$$x_0 = [3 \quad 1]^{\mathrm{T}}, \quad \hat{x}_0 = [0.1 \quad 4.5]^{\mathrm{T}},$$
$$P_{x_0} = \begin{bmatrix} 36 & 0 \\ 0 & 36 \end{bmatrix}, \quad R_v = 10^{-6} \begin{bmatrix} 1 & 0 \\ 0 & 1 \end{bmatrix},$$
$$R_n = 10^{-2} \begin{bmatrix} 1 & 0 \\ 0 & 1 \end{bmatrix}.$$

The estimation result for the unconstrained case is shown in Fig. 10. The result shows that the dynamic performance of the UKF estimates is better compared to that of the EKF. The EKF performance is very similar to the reported results in [14].

However, during the dynamic response, both the UKF and EKF estimates become negative, (meaning negative concentrations) which is not possible physically. State constraints are incorporated according to the proposed method in Section 3 for the UKF and standard "clipping" is used for the EKF. The results are shown in Fig. 11. From Fig. 11 the UKF estimates converge to the true states without violating the constraints. Because of the clipping in the

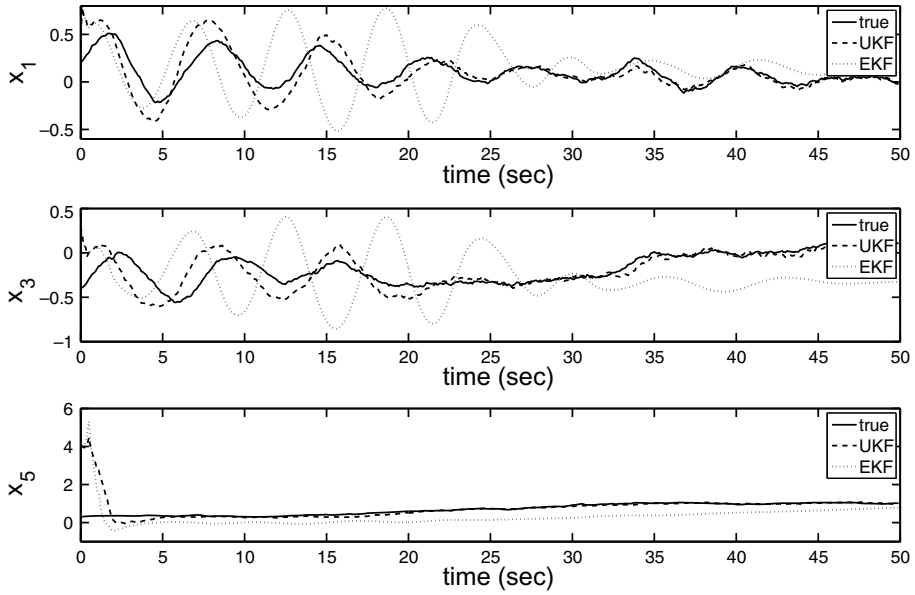

Fig. 9. Comparison of estimated states: components of stator flux.

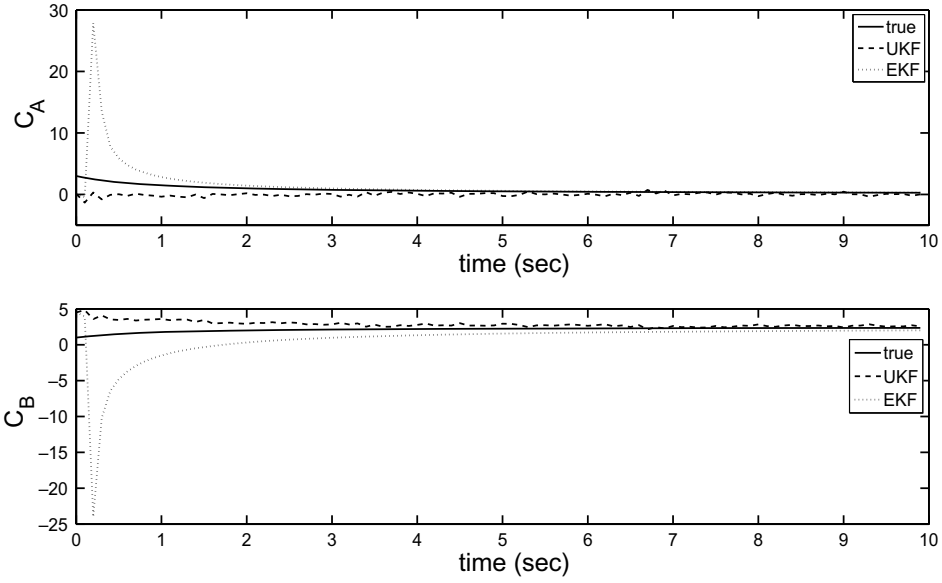

Fig. 10. Comparison of estimated states: no constraint handling.

EKF, C_A estimate of EKF did not converge to the true state and the estimate of C_B takes much longer time to converge to the true state.

Fig. 12 shows the phase portraits of the unconstrained and constrained UKF estimates for the first 4 s. The figure also includes the corresponding covariances plotted at $t = 0$, 1 and 3 s. From Fig. 12, it is clear that it takes longer time for the unconstrained estimate to converge as the corresponding covariances do no include the constraint information. The constrained UKF estimate converges faster as the covariances decrease faster, which include the constraint information. The results from this example confirm that the proposed constraint handling method is promising.

4.4. SOFC/GT hybrid system

The solid oxide fuel cell (SOFC) stack integrated in a gas turbine (GT) cycle, known as SOFC/GT hybrid system, is an interesting power generation system due to its high efficiency in the range of 65–75%. A schematic diagram of the SOFC/GT hybrid system integrated in an autonomous power system is shown in Fig. 13. The fuel, natural gas (CH_4), is partially steam reformed in a pre-reformer before

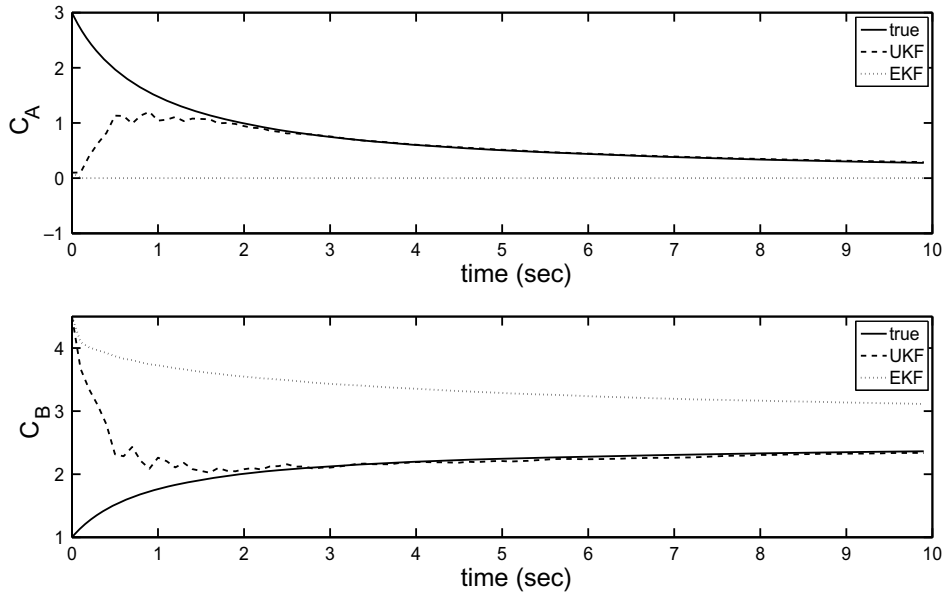

Fig. 11. Comparison of state estimates: state constraint handling.

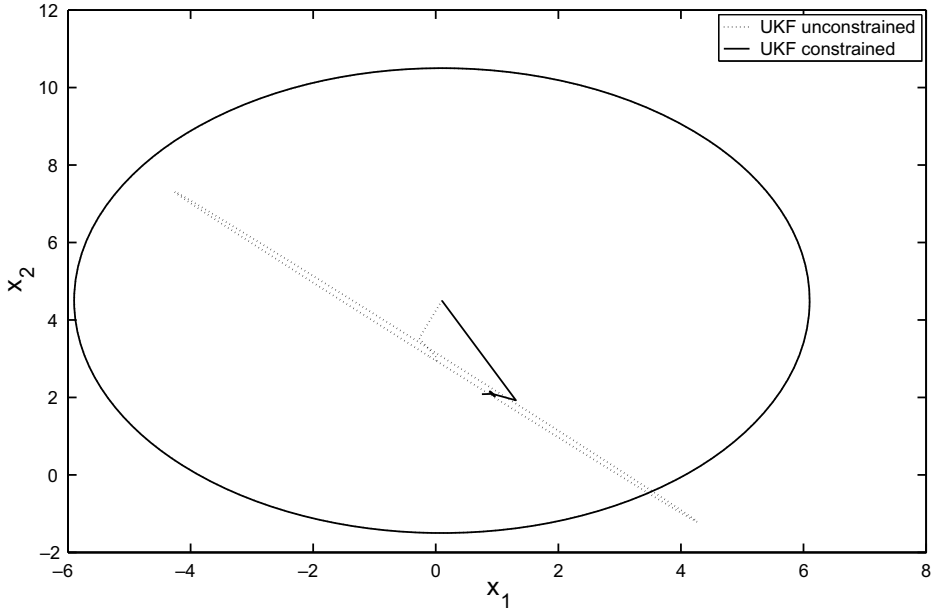

Fig. 12. Phase portraits of the UKF unconstrained and constrained estimates with covariances.

it enters the SOFC anode. A part of anode flue gas is recycled to supply the necessary steam required for the steam reformation in the pre-reformer. The remaining part of the anode flue gas is supplied to a combustor where the unused fuel is burnt completely in presence of oxygen coming from the cathode flue gas. Air is compressed and preheated in a heat exchanger before entering the SOFC cathode. The hot stream from the combustor is expanded using a high pressure turbine (HPT) which drives the compressor. The HPT flue gas is expanded to atmospheric pressure using low pressure turbine (LPT) which drives an alternator. The DC power from SOFC stack is inverted to AC using an inverter. The inverter and the alternator are connected to the electric load through a bus bar. Typically 60–70% of the total power is supplied by the SOFC stack.

All the models of the system are developed in the modular modeling environment gPROMS [7] as reported in [5]. In [5], a low complexity, control relevant SOFC model is evaluated against a detailed model developed in [6]. The comparisons indicate that the low complexity model is sufficient to approximate the important dynamics of the

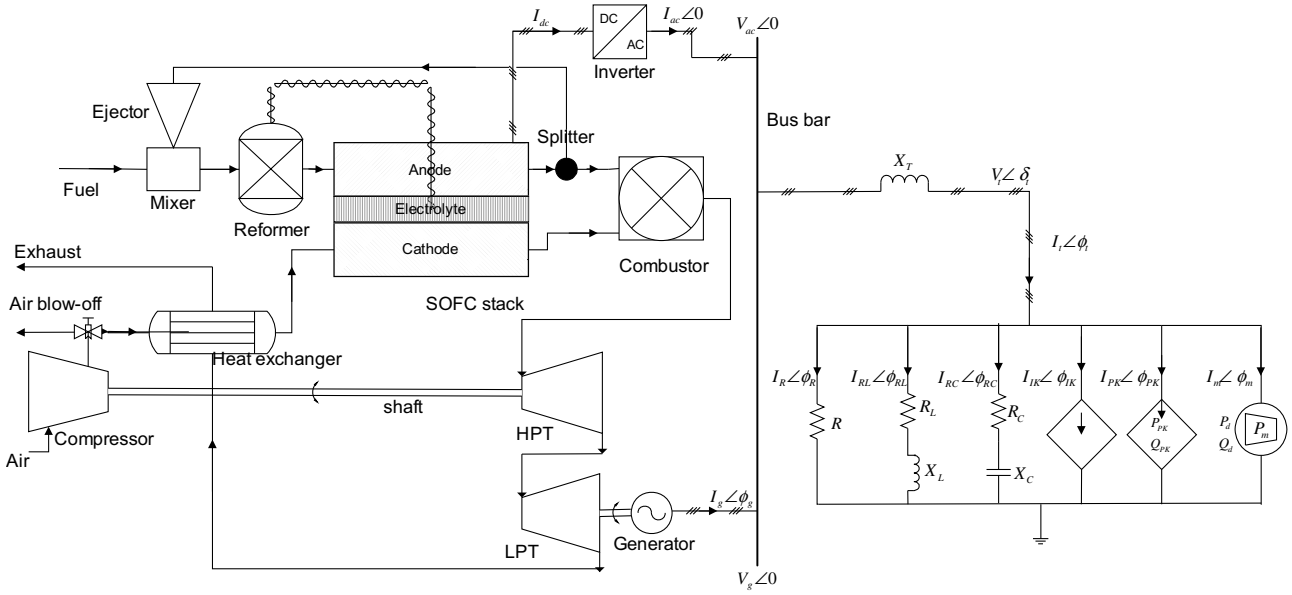

Fig. 13. SOFC-GT hybrid system integrated in an autonomous power system.

SOFC and can hence be used for operability and control studies. A regulatory control layer is designed and it is included in the model.

The purpose of a state estimator is to design an advanced controller and as well for monitoring and fault diagnosis purposes. In this section, EKF and UKF are used to design the state estimator, and their performances and computational load are compared.

The SOFC/GT hybrid system model has 3 inputs, 18 states, and 14 measured outputs which are listed in Table 2. A state estimator of the hybrid system is designed using both the UKF and EKF, and the simulation results are presented in Figs. 14 and 15. The figures show selected states for a typical run. Both the state estimators are tuned to obtain good performance. In the EKF, the Jacobians are calculated numerically at each time step. The tuning parameters for both the UKF and EKF are the same to ensure a fair comparison.

The initial state estimate is different from the actual initial state and from the simulation results it can be concluded that UKF estimate converges to the true states very fast compared to the EKF estimate. The initial state estimate cannot be chosen too far from the actual state to avoid numerical problems in gPROMS. From this example, it is clear that the UKF can be used to design state estimators for higher order systems and the UKF performance is again favorable. The computational load of the UKF is almost the same as that of the EKF, in addition to providing better performance.

Table 2
Available measurements

No.	Measurement
1	Pre-reformer temperature (K)
2	Shaft speed (rad/s)
3	Heat exchanger hot stream temperature (K)
4	Heat exchanger cold stream temperature (K)
5	SOFC outlet temperature (K)
6	Combustor outlet temperature (K)
7	Fuel mass flow rate (kg/s)
8	Anode recycle flow rate (kg/s)
9	Flow to the combustion chamber (kg/s)
10	Air blow-off flow rate (kg/s)
11	Air mass flow rate (kg/s)
12	SOFC current (A)
13	SOFC voltage (V)
14	Generator power (kW)

5. Discussion

The UKF as a tool for state estimation has been compared to the standard method for nonlinear state estimation; the EKF. The state estimation methods have been compared using the same tuning parameters to make the comparative study as credible as possible. Four different examples have been tested. The UKF shows consistently improved performance as compared to the EKF. In several cases the improvement is substantial, both in the convergence rate as well as in the long term state estimation error. Monte Carlo simulations have also been run with different initial states. These runs reinforced the hypothesis that the UKF is indeed an interesting alternative to the EKF.

A method for constraint handling in UKF is proposed in Section 3. The results albeit for one example are promising. An important feature of the proposed constraint handling method is the fact that it adjusts the covariance in addition to the state estimates themselves. This is quite different from the EKF where 'clipping' usually is performed without adjusting the state estimate covariance. A rationale for using the MHE is often attributed to its constraint handling ability. Our results indicate that the UKF with the proposed constraint handling may be an interesting alter-

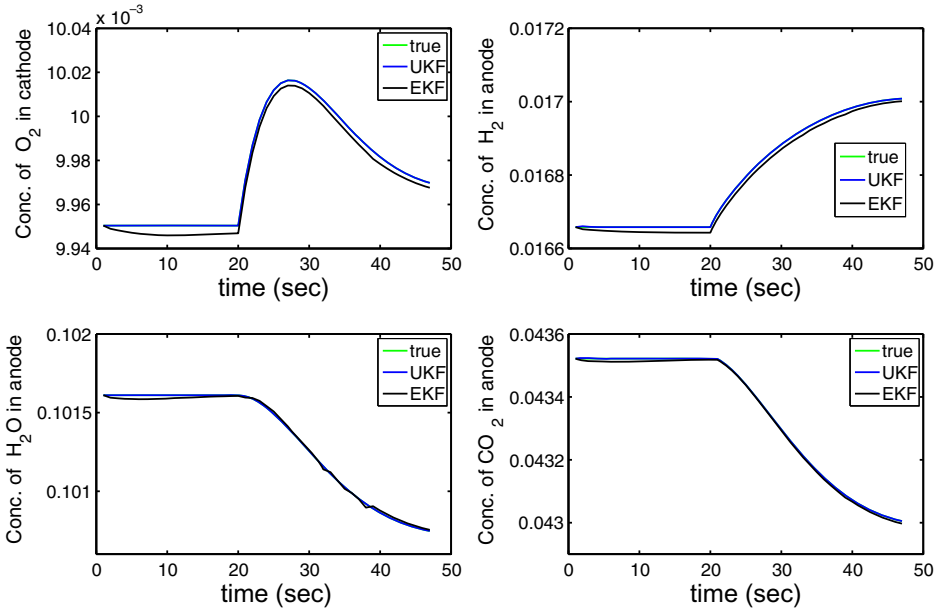

Fig. 14. Comparison of state estimation using UKF and EKF: concentration of O_2 in cathode and concentrations of H_2, H_2O and CO_2 in anode of SOFC.

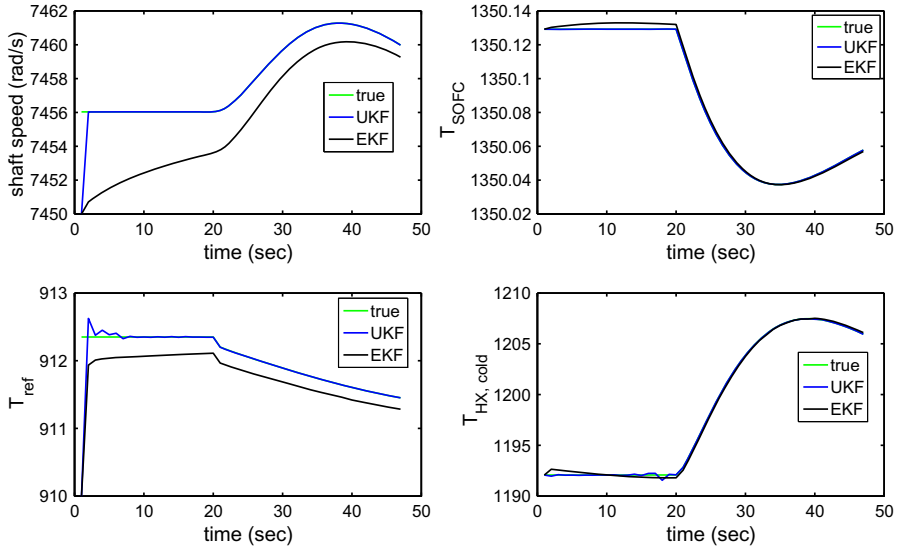

Fig. 15. Comparison of state estimation using UKF and EKF: Compressor shaft speed and SOFC, prereformer and heat exchanger cold stream temperatures.

native to MHE. Furthermore, it is very simple to implement the proposed method to incorporate the constraints in the UKF compared to the MHE.

The improved performance of the UKF compared to the EKF is due to two factors, the increased time-update accuracy and the improved covariance accuracy. The covariance estimation can be quite different for the two filters as shown in Fig. 6. This again makes a difference in terms of different Kalman gains in the measurement-update equation and hence the efficiency of the measurement-update step.

There is usually a price to pay for improved performance. In this case the computational load increases when moving from the EKF to the UKF if the Jacobians are computed analytically. In many cases, particularly for higher order systems, the Jacobians for the EKF are computed using finite differences. In this case the computational load for the UKF is comparable to the EKF. The latter implies that the computational load using the UKF is significantly lower than what can be expected for the MHE.

6. Conclusions

This paper shows that the UKF is an interesting option to the EKF because of improved performance. Further,

due to the proposed constraint handling method it may also be an interesting alternative to the MHE. The proposed method is much simpler to implement compared to the MHE. The computational load for the UKF is comparable to the EKF for the typical case, where the Jacobians are computed numerically.

Acknowledgements

The authors are grateful to Professor Biao Huang for discussions on the UKF. The financial support from The Gas Technology Center, NTNU-SINTEF and Norwegian Research Council is acknowledged. Further the financial support from the NFR BIGCO2 project is also acknowledged.

References

[1] S. Julier, J.K. Uhlmann, Unscented filtering and nonlinear estimation, Proceedings of the IEEE 92 (2004) 401–422.
[2] C.T. Chen, Linear System Theory and Design, Oxford University Press, New York, 1999.
[3] L. Salvatore, S. Stasi, L. Tarchioni, A new EKF-based algorithm for flux estimation in induction machines, IEEE Transactions on Industrial Electronics 40 (5) (1993) 496–504.
[4] K. Reif, F. Sonnemann, R. Unbehauen, An EKF-based nonlinear observer with a prescribed degree of stability, Automatica 34 (9) (1998) 1119–1123.
[5] R. Kandepu, L. Imsland, B. Foss, C. Stiller, B. Thorud, O. Bolland, Modeling and control of a SOFC-GT based autonomous power system, Journal of Energy 2006 36 (2007) 406–417.
[6] C. Stiller, B. Thorud, S. Seljbeo, H. Karoliussen, O. Bolland, Finite-volume modeling and hybrid-cycle performance of planar and tubular solid oxide fuel cells, Journal of Power Sources 141 (2005) 227–240.
[7] gPROMS, gPROMS introductory user guide, Process Systems Enterprise Ltd, 2004.
[8] R. Van der Merwe, Sigma-Point Kalman Filters for probability inference in dynamic state-space models, PhD Thesis, Oregon Health and Science University, 2004.
[9] B. Huang, Q. Wang, Overview of emerging Bayesian approach to nonlinear system identification, in: Round Tables on Non-linear Model Identification, International Workshop on Solving Industrial Control and Optimization Problems, Cramado, Brazil, April 6–7, 2006.
[10] G. Evensen, Data Assimilation, The Ensemble Kalman Filter, Springer, Berlin, 2007.
[11] A.H. Jazwinski, Stochastic Processes and Filtering Theory, Mathematics in Science and Engineering, vol. 64, Academic Press, New York and London, 1970.
[12] H.K. Khalil, Nonlinear Systems Third Edition, Prentice Hall, 2000.
[13] M.S. Ahmed, S.H. Riyaz, Design of dynamic numerical observers, IEE Proceedings – Control Theory and Applications 147 (3) (2000) 257–266.
[14] E.L. Haseltine, J.B. Rawlings, A critical evaluation of extended kalman filtering and moving horizon estimation, Technical Report, Texas-Wisconsin Modeling and Control Consortium (TWMCC), 2002–2003.
[15] A. Romanenko, J.A.A.M. Castro, The unscented filter as an alternative to the EKF for nonlinear state estimation: a simulation case study, Computer and Chemical Engineering 28 (2004) 347–355.
[16] B. Akin, U. Orguner, Aydin Ersak, State estimation of induction motor using unscented Kalman filter, IEEE Transactions on Control Applications 2 (2003) 915–919.
[17] C.V. Rao, J.B. Rawlings, D.Q. Mayne, Constrained state estimation for nonlinear discrete-time systems: stability and moving horizon approximations, IEEE Transactions on Automatic Control 48 (2003) 246–258.
[18] D. Simon, T.L. Chia, Kalman filtering with state equality constraints, IEEE Transactions on Aerospace and Electronic Systems 38 (2002) 128–136.
[19] S. Ungarala, E. Dolence, K. Li, Constrained extended kalman filter for nonlinear state estimation, in: Proceedings of 8th International IFAC Symposium on Dynamics and Control Process Systems, Cancun, Mexico, June 2007, vol. 2, pp. 63–68.
[20] W. Li, H. Leung, Simultaneous registration and fusion of multiple dissimilar sensors for cooperative driving, IEEE Transactions on Intelligent Transportation Systems 5 (2004) 84–98.